Cerebral Cortex, November 2020;30: 5943–5959

doi: 10.1093/cercor/bhaa168
Advance Access Publication Date: 18 June 2020
Original Article

ORIGINAL ARTICLE

Altered Resting-State Functional Connectivity Between Awake and Isoflurane Anesthetized Marmosets

Yuki Hori[1,†], David J. Schaeffer[1,†], Kyle M. Gilbert[1], Lauren K. Hayrynen[1], Justine C. Cléry[1], Joseph S. Gati[1], Ravi S. Menon[1] and Stefan Everling[1,2]

[1]Centre for Functional and Metabolic Mapping, Robarts Research Institute, The University of Western Ontario, London, Ontario N6A 5B7, Canada and [2]Department of Physiology and Pharmacology, The University of Western Ontario, London, Ontario N6A 5C1, Canada

Address correspondence to Stefan Everling, PhD, Centre for Functional and Metabolic Mapping, Robarts Research Institute, The University of Western Ontario, London, Ontario N6A 5B7, Canada. Email: severlin@uwo.ca.

[†]Y.H. and D.J.S. have equally contributed to this work and are co-first authors.

Abstract

The common marmoset (*Callithrix jacchus*) is a New World primate that is becoming increasingly popular as a preclinical model. To assess functional connectivity (FC) across the marmoset brain, resting-state functional MRI (RS-fMRI) is often performed under isoflurane anesthesia to avoid the effects of motion, physiological stress, and training requirements. In marmosets, however, it remains unclear how isoflurane anesthesia affects patterns of FC. Here, we investigated the effects of isoflurane on FC when delivered with either medical air or 100% pure oxygen, two canonical methods of inhalant isoflurane anesthesia delivery. The results demonstrated that when delivered with either medical air or 100% oxygen, isoflurane globally decreased FC across resting-state networks that were identified in awake marmosets. Generally, although isoflurane globally decreased FC in resting-state networks, the spatial structure of the networks was preserved. Outside of the context of RS networks, we indexed pair-wise functional connectivity between regions across the brain and found that isoflurane substantially altered interhemispheric and thalamic FC. Taken together, these findings indicate that RS-fMRI under isoflurane anesthesia is useful to evaluate the global structure of functional networks, but may obfuscate important nodes of some network components when compared to data acquired in fully awake marmosets.

Key words: default mode network, isoflurane, marmoset, resting-state functional MRI, thalamus

Highlights

- We show differences of functional networks in marmosets between anesthetized and awake conditions.
- Isoflurane globally decreases cortical FC across resting-state networks.
- Isoflurane substantially alters thalamic and interhemispheric FC.

Introduction

The common marmoset (*Callithrix jacchus*) is becoming increasingly popular as a preclinical animal model. Despite having a similar body size to a rat, marmosets as primates have a cortical organization more similar to humans (Okano and Mitra 2015). Additionally, marmosets are more amenable to transgenic techniques than macaque monkeys given their reproductive efficiency and early sexual maturity (12–18 months) (Sasaki et al. 2009; Park et al. 2016; Tomioka, Ishibashi, et al. 2017a; Tomioka, Nogami, et al. 2017b). In addition, the lissencephalic

(smooth) marmoset cortex offers the opportunity for laminar electrophysiological recordings (Johnston et al. 2019) and calcium imaging in many cortical areas (Yamada et al. 2016; Ebina et al. 2018; Kondo et al. 2018). Thus, the common marmoset holds tremendous promise as a nonhuman primate model for translational neuroscience (T'Hart et al. 2013; Hashikawa et al. 2015; Miller et al. 2016; Mitchell and Leopold 2015).

A rapidly growing body of research uses resting-state functional magnetic resonance imaging (RS-fMRI) in nonhuman primates to examine brain organization and function for cross-species comparisons. While humans are usually awake for RS-fMRI experiments, a majority of RS-fMRI studies in non-human primates use anesthetic agents to avoid the effects of motion, physiological stress, and training requirements (Milham et al. 2020). Several studies have revealed the effects of anesthesia on functional networks in humans (Peltier et al. 2005; Greicius et al. 2008; Boveroux et al. 2010; Deshpande et al. 2010; Martuzzi et al. 2010), macaques (Vincent et al. 2007; Hutchison et al. 2014; Barttfeld et al. 2015; Uhrig et al. 2018), and rodents (Liu et al. 2011; Liu, Pillay, et al. 2013b; Grandjean et al. 2014; Paasonen et al. 2018). These studies have shown anesthesia-induced changes of the strength of the network/connectivity by anesthesia, but there has been less focus on the overall structure of these networks. Additionally, in marmosets, there is only one report detailing the difference between fMRI under anesthetized and awake conditions (Liu, Hirano, et al. 2013a); however, this report focused on the effects of propofol anesthesia on the blood-oxygen-level dependent (BOLD) signal and functional connectivity related to somatosensory stimulation. Here, we investigated the effects of isoflurane, an inhalant anesthesia that is commonly used for non-human primate RS-fMRI because of its suitability for survival studies, rapid induction and recovery, low cost, and the nonobligatory requirement for mechanical ventilation (Vincent et al. 2007; Shmuel and Leopold 2008; Hutchison et al. 2011, 2014; Mars et al. 2011; Sadagopan et al. 2015; Ghahremani et al. 2016; LaClair et al. 2019; Schaeffer, Gilbert, Gati, et al. 2019a; Schaeffer, Gilbert, Ghahremani, et al. 2019b; Hori et al. 2020).

Non-human primate RS-fMRI studies that use isoflurane anesthesia often do so in combination with 100% oxygen (Ghahremani et al. 2016; Schaeffer, Gilbert, Gati, et al. 2019a; Schaeffer, Gilbert, Ghahremani, et al. 2019b; Hori et al. 2020). It has been shown, however, that altering the concentration of oxygen in the breathing gas (i.e., compared to 21% oxygen in room air) may also affect FC by way of altering cerebrovascular reactivity (Buxton 2010; Gagnon et al. 2015). This is potentially problematic with the fMRI signal being sensitized to detect differences in blood oxygenation (Ogawa et al. 1990). As such, the effect of isoflurane on RS-fMRI network connectivity could by further confounded by the makeup of the breathing gas through which it is delivered. One way to circumvent this potentially interactive effect is to deliver isoflurane using medical air, which has the same oxygen concentration as room air (but is filtered of impurities). Here, we disentangle the effects of isoflurane and oxygen concentration on resting-state networks canonically identified in marmoset monkeys (Belcher et al. 2013, 2016; Schaeffer, Gilbert, Hori et al. 2019c). Although there is evidence that isoflurane anesthesia seems to affect network connectivity at a broad and global level in other primate species (Hutchison et al. 2014), it is likely that this effect is downstream from the known regional effects of anesthetic agents. For example, sevoflurane can substantially reduce thalamic activity at doses that cause sedation (for a review see Alkire et al. 2008), while isoflurane has been shown to attenuate the output of somatosensory signals in the thalamic nucleus in rats (Detsch et al. 1999), and ketamine increases the global metabolism in humans especially in the thalamus (Peltier et al. 2005; Greicius et al. 2008; Boveroux et al. 2010; Deshpande et al. 2010; Martuzzi et al. 2010). As such, in addition to comparing networks at a network level (i.e., those identified using independent component analyses), we also compared FC at a regional level via pair-wise comparisons of BOLD time courses—this allowed for assessment of regional effects, particularly FC of thalamus with the rest of the brain.

We had three primary objectives: 1) To isolate resting-state networks using fully-awake data, allowing for corroboration of previously identified networks in marmosets using RS-fMRI (Belcher et al. 2013), but with our fMRI hardware and acquisition protocols. 2) Determine how the strength and structure of these networks differed between marmosets who were fully awake or anesthetized with 1.5% isoflurane delivered in either medical air or 100% oxygen. 3) Identify regionally specific effects of isoflurane, with a specific focus thalamic connectivity. It is worth noting that dose-dependent effects of isoflurane have been shown in macaques (Hutchison et al. 2014), but given that such high doses of isoflurane are unlikely to be used in functional imaging studies in marmosets, we chose to focus on the canonically used isoflurane concentration of 1.5%. We expect that our findings will be informative to those interested in using marmosets to model alterations in resting state functional networks as a means to study human brain pathologies.

Materials and Methods

Animal Preparation

All surgical and experimental procedures were in accordance with the Canadian Council of Animal Care policy and a protocol approved by the Animal Care Committee of the University of Western Ontario Council on Animal Care. Five common marmosets (one female; 323 ± 61 g; 1.6 ± 0.3 years old at the beginning of awake experiments) were used in this study. MRI experiments were performed under three conditions: fully awake, isoflurane anesthesia with medical air (Iso + Med), and isoflurane anesthesia with 100% oxygen (Iso + O_2). Among the five monkeys, two were scanned under all three conditions. Of the remaining three monkeys, two were scanned under awake and Iso + Med conditions. The remaining monkey was scanned under awake and Iso + O_2 conditions. Thus, the number of subjects were five for awake, four for Iso + Med, and three for Iso + O_2. Before the MRI experiments, all marmosets underwent an aseptic surgery to implant a head chamber to fix the head during MRI acquisition as described in previous reports (Johnston et al. 2018; Schaeffer, Gilbert, Hori et al. 2019c). Briefly, the marmoset was placed in a stereotactic frame (Narishige Model SR-6C-HT), and a chamber was attached to the skull using several coats of adhesive resin (All-bond Universal Bisco, Schaumburg, Illinois, USA), and a dental cement (C & B Cement, Bisco, Schaumburg, Illinois, USA) using a stereotactic manipulator to ensure correct location and orientation. The chamber was 3D printed at 0.25-mm resolution using stereolithography and a clear photopolymer resin (Clear-Resin V4; Form 2, Formlabs, Somerville, Massachusetts, USA).

Imaging Hardware and Acquisition Parameters

The hardware and the acquisition parameters were identical for all marmosets in both awake and anesthetized conditions. Data

were acquired using a 9.4-T 31-cm horizontal bore magnet (Varian/Agilent, Yarnton, UK) and Bruker BioSpec Avance III console with the software package Paravision-6 (Bruker BioSpin Corp, Billerica, MA), a custom-built high-performance 15-cm-diameter gradient coil with 400-mT/m maximum gradient strength (Peterson et al. 2018), and a 5-channel receive coil (Schaeffer, Gilbert, Hori et al. 2019c). Radiofrequency transmission was accomplished with a quadrature birdcage coil (12-cm inner diameter) built in-house. All imaging was performed at the Centre for Functional and Metabolic Mapping at the University of Western Ontario.

For all conditions, functional images were acquired with 6 functional runs (at 600 volumes each) for each animal in separate sessions, using a gradient-echo based single-shot echo-planar imaging sequence with the following parameters: TR = 1500 ms, TE = 15 ms, flip angle = 40°, field of view (FOV) = 64 × 64 mm, matrix size = 128 × 128, voxel size = 0.5 mm isotropic, slices = 42, bandwidth = 500 kHz, generalized autocalibrating parallel acquisition (GRAPPA) acceleration factor (anterior-posterior) = 2. A T2-wighted image (T2w) was acquired for each animal using rapid imaging with refocused echoes (RARE) sequences with the following parameters: TR = 5500 ms, TE = 53 ms, FOV = 51.2 × 51.2 mm, matrix size = 384 × 384, voxel size = 0.133 × 0.133 × 0.5 mm, slices = 42, bandwidth = 50 kHz, GRAPPA acceleration factor (anterior–posterior) = 2.

Animal Training

Before MRI acquisition, the marmosets were first acclimatized to the animal holder, head fixation system, and a mock MRI environment prior to the first imaging session (Silva et al. 2011). Each marmoset was trained over the course of 3 weeks. During the first week, marmosets entered the tube and were constrained using only the neck and tail plates for increasingly long periods of time (up to 30 min). During the second week, the restraint tube was inserted into a mock MRI bore (a 12-cm inner diameter tube) to simulate the scanner environment; MRI sounds were played at increasingly loud volumes (up to 80 dB) for increasingly long durations, up to 60-min sessions. In week 3, marmosets were head fixed via the fixation pins, inserted into the mock MRI tube and exposed to the MRI sounds. Within each session, the animals are presented with reward items (pudding or marshmallow fluff) for remaining still (calmly facing forward, with minimal movement of limbs). Throughout the training sessions, the behavioral rating scale described by Silva et al. (2011) was used to assess the animals' tolerance to the acclimatization procedure. By the end of week 3, all five marmosets scored 1 or 2 on this assessment scale (Silva et al. 2011), showing calm and quiet behavior, with little signs of agitation.

Imaging Acquisition Under Awake Condition

For awake experiments, all five marmosets were restrained in the animal holder using a neck plate and a tail plate. The animal was then head fixed using fixation pins in the MRI room to minimize the time in which the awake animal was head fixed (Schaeffer, Gilbert, Hori et al. 2019c). This head-fixation system allows for the collection of RS-fMRI with little to no head movement (Schaeffer, Gilbert, Hori et al. 2019c). Indeed, maximum head translation in each scan (15 min) ranged from 30 to 81 μm for awake, and 18 to 77 μm for anesthetized monkeys, respectively. Once fixed, a lubricating gel (MUKO SM321N, Canadian Custom Packaging Company, Toronto, Ontario, Canada) was squeezed into the chamber and applied to the brow ridge to reduce the magnetic susceptibility artifacts (see Schaeffer, Gilbert, Hori et al. 2019c for differences without gel).

Imaging Acquisition Under Anesthetized Condition

Anesthetized data were acquired at least 1 week after completing awake experiments to avoid the alteration of cerebrovascular reactivity and cerebral blood flow by anesthesia (Wegener and Wong 2008). Animals were initially sedated with an intramuscular injection of ketamine (20 mg/kg). After the animal was positioned in the animal holder in the same manner as the awake procedure, anesthesia was maintained using inhalation of 1.5% isoflurane with medical air or 100% oxygen through a custom anesthesia mask (computer aided design file in Schaeffer, Gilbert, Hori et al. 2019c). During scans, a veterinary technician monitored respiration rate, saturation of percutaneous oxygen (SpO_2), and heart rate via pulse oximeter and observed these values to be within a normal range throughout scans. Body temperature was also measured and maintained using warm-water circulating blankets, thermal insulation, and warmed air.

Image Preprocessing

Data were preprocessed using FSL software (Smith et al. 2004). Raw MRI images were first converted to Neuro Informatics Technology Initiative (NIfTI) format (Li et al. 2016) and reoriented from sphinx position. Brain masks were created using FSL tools and the National Institutes of Health (NIH) T2w brain template (Liu et al. 2018), which has only the brain (as it is *ex vivo*, without a skull). For each animal, the brain-skull boundary was first roughly identified from individual T2w images using the brain extraction tool (BET) with the following options: radius of 25–40 mm and fractional intensity threshold of 0.3 (Smith 2002). Then, the NIH T2w brain template was linearly and non-linearly registered to the individual brain image using FMRIB's linear registration tool (FLIRT) and FMRIB's nonlinear registration tool (FNIRT) to more accurately create the brain mask. After that, the brain was extracted using the brain mask. RS-fMRI images in both conditions were corrected for motion using FLIRT. Principal component analysis (PCA) was applied to remove the unstructured noise from the RS-fMRI time course, followed by independent component analysis (ICA) with the decomposition number of 200 using Multivariate Exploratory Linear Optimized Decomposition into the Independent Components (MELODIC) module of the FSL software package. Obtained components were classified as signal or noise (such as eye movement, cerebrospinal fluid (CSF) pulsation, heart rate, and respiratory artifacts) based on the criteria as shown in a previous report (Griffanti et al. 2017), and noise components were regressed out from the RS-fMRI time course using FSL tool (fsl_regfilt). All RS-fMRI images were finally normalized to the NIH template using RS-fMRI-to-T2w and T2w-to-template transformation matrices obtained by FLIRT and FNIRT, followed by spatial smoothing by Gaussian kernel with the full-width of half-maximum value of 1.0 mm.

Dual Regression Analysis

To quantitatively compare the resting-state functional networks between awake and anesthetized conditions, we used a dual regression technique that allows for voxel-wise comparisons of resting-state functional maps (Filippini et al. 2009). First, the concatenated awake RS-fMRI data sets were decomposed using

MELODIC to identify large-scale patterns of FC to be applied as spatial templates for the dual regression approach. Because we focus on evaluating isoflurane-induced changes from baseline, the anesthetized RS-fMRI data was not included in the calculation of the spatial templates. The ICA analysis was implemented 10 times with different dimension numbers (from 16 to 25) to identify optimal dimensionality—the 20-component solution was selected to be an appropriate representative of meaningful components with reference to previous reports of marmoset functional networks (Belcher et al. 2013; Ghahremani et al. 2016). Second, the dual-regression approach was used to identify the scan-specific temporal dynamics and associated spatial maps within each scan's fMRI data sets. This process involves 1) using the full set of group-ICA spatial templates in a linear model fit against the separate fMRI data sets, resulting in matrices describing temporal dynamics for each component and scan (spatial regression), and 2) using these time-course matrices in a linear model fit against the associated fMRI data set to estimate scan-specific spatial maps (temporal regression). Finally, the different component maps across scans were tested for significant differences of amplitude between conditions using nonparametric permutation testing (5000 permutations; FSL's Randomize). This resulted in spatial maps characterizing the inter-condition differences. $P < 0.05$ was considered as significantly differences between awake and anesthetized conditions.

Calculation of Functional Connectivity

All RS-fMRI images for each condition were concatenated and parcellated based on the Paxinos Atlas (Liu et al. 2018). The mean time signals for each region were obtained by averaging the fMRI time series across all voxels contained within the volume-of-interest (VOI), then correlation coefficients between all regions were calculated. To identify the strength of FC from the left and right thalamus at the voxel level, we also calculated seed-by-voxel FC maps using the FEAT tool of the FSL software package (Smith et al. 2004). Given that the we did not have sufficient signal to noise ratio (SNR) to evaluate the FC between each thalamic nucleus and the rest of the brain, we used a larger VOI in the thalamus (70.75 mm^3 per hemisphere) included multiple areas, anterior, laterodorsal, mediodorsal, ventral anterior, ventral lateral, ventral posterior thalamic nuclei and pulvinar. The time courses from the left and right thalamus were extracted for each scan after normalization to a T2-weighted template, and correlation maps (z-score maps) with left and right thalamus were calculated using FEAT. Here, the strength of FC was defined as the z-value. The average FC maps across scans were presented on the surface map using the Connectome Workbench (Marcus et al. 2011). The mean FC values for each VOI were obtained by averaging the FC values across all voxels contained within the VOI; thalamic connections where there was a significant difference between awake and anesthetized conditions were identified using paired-sample *t*-tests. Bonferroni correction was used to counteract the problem of multiple comparisons, with $P < 0.01$.

Results

Identification of Resting-state Networks

After implementation of group ICA using only the awake RS-fMRI data, eight components were identified as unstructured and/or physiological noise based on the following criteria: 1) there was no activation higher than z-values of 3.1; 2) there was main activation in the vein or cerebrospinal fluid (CSF); 3) there were only unilateral activation patterns except for visual components. The remaining 12 components demonstrated meaningful neural functional networks. These networks were thresholded at $z = 3.1$ for visual purposes. Cytoarchitectonic borders based on the Paxinos atlas (Liu et al. 2018) and abbreviations used in this study are summarized in Figure 1A–D. The following resting-state networks (RSNs) were consistent with known RSNs in previous reports (Belcher et al. 2013; Ghahremani et al. 2016; Schaeffer, Gilbert, Hori et al. 2019c); default mode, attention, ventral somatomotor, dorsal somatomotor, medial somatomotor, salience, primary visual (left and right), anterior high-order visual, dorsal high-order visual, ventral high-order visual, and basal ganglia networks (Fig. 1E).

Comparison of Functional Networks

These 12 functional networks were used as templates to evaluate the differences between awake and anesthetized resting-state networks by dual regression. Figures 2 and 3 show the differences of functional coactivation areas between awake and Iso + Med conditions. The bottom rows in each component indicate *P*-value images, showing areas with significantly reduced functional connectivity in the anesthetized compared with the awake condition. Isoflurane decreased the strength of coactivation in the cortical networks, but the structures of these networks were preserved by 1.5% isoflurane anesthesia. These findings were consistent with the results of a previous macaque study (Hutchison et al. 2014). A notable difference was the default mode network, which lacked activation in lateral frontal cortex (area 8aD) in the anesthetized condition (Fig. 2A).

Figures 4 and 5 show the differences of functional coactivation areas between awake and Iso + O_2 conditions. The results were similar as for the comparison between the awake and Iso + Med conditions. Isoflurane in combination with 100% oxygen also decreased the strength of coactivation in the cortical networks, but the overall structure of most networks was preserved. The only exception was again default mode network, which lacked the frontal component in the anesthetized condition (Fig. 4A).

The Effects of Isoflurane on Correlation Coefficients Among Seed Regions

The matrices of correlation coefficients (CCs) for awake and anesthetized marmoset VOIs are shown in Figure 6A–C. In the awake condition, both left and right hemispheres had strikingly similar intracortical patterns and there were patterns of strong connectivity with the contralateral hemisphere for multiple areas (Fig. 6A). In contrast, interhemispheric correlations were decreased by anesthesia (both Iso + Med and Iso + O_2 conditions), while intrahemispheric correlations were relatively preserved (Fig. 6B and C). This tendency was consistent with a previous macaque study that showed dose-dependent reduction of interhemispheric correlations (Hutchison et al. 2014). The regression lines between awake and Iso + Med were expressed as $CC(Iso + Med) = 0.49 \times CC(Awake) + 0.085$ for intrahemispheric correlations, and $CC(Iso + Med) = 0.37 \times CC(Awake) + 0.054$ for interhemispheric correlations, respectively (Fig. 6D). There was a significant difference between slopes of these regression lines (analysis of covariance (ANCOVA): $P < 0.001$). The regression lines between awake and Iso + O_2 were expressed as $CC(Iso + O_2) = 0.43 \times CC(Awake) + 0.066$ for intra-hemispheric

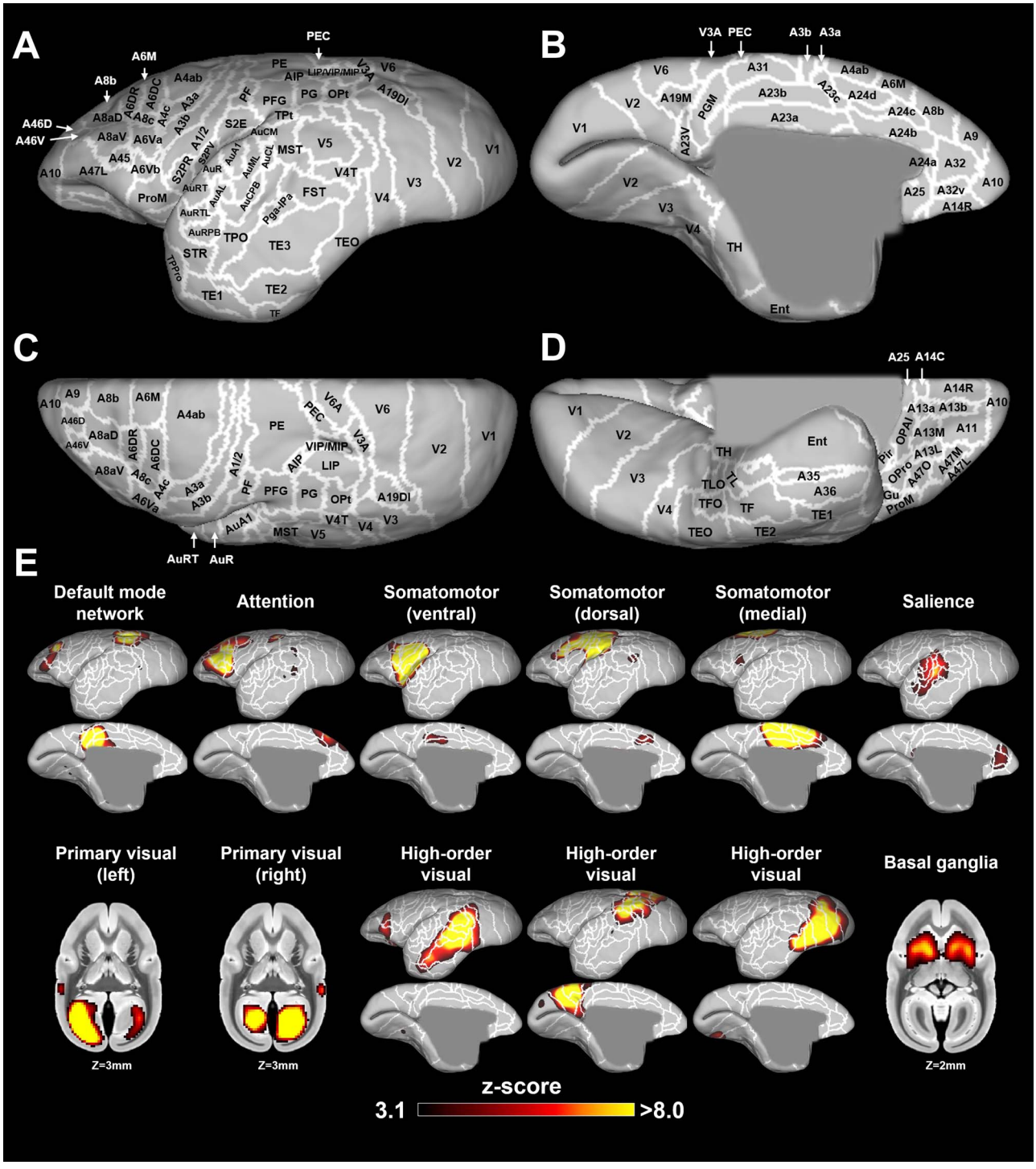

Figure 1. Cytoarchitectonic borders based on the Paxinos atlas (Liu et al. 2018) in lateral (*A*), medial (*B*), dorsal (*C*), and ventral (*D*) views. *E* shows the resting-state functional networks obtained by independent component analysis (ICA) in the awake condition. Twelve networks are shown as thresholded *z*-score maps on the NIH surface (only left hemisphere) or volume atlases. White lines show cytoarchitectonic borders, for reference (Liu et al. 2018).

correlations, and $CC(Iso + O_2) = 0.20 \times CC(Awake)$—0.011 for interhemispheric correlations, respectively (Fig. 6*E*). There was also a significant difference between slopes of these regression lines (ANCOVA: $P < 0.001$). These results indicate that isoflurane anesthesia decreases interhemispheric correlations more than intra-hemispheric correlations. The distributions of the correlation coefficients during awake and anesthetized conditions were shown in Figure 6*F*–*I*. The interhemispheric connections with correlation coefficients of over 0.5 were dramatically decreased in both anesthetized conditions (Fig. 6*G* and *I*), while intra-hemispheric connections were preserved (Fig. 6*F* and *H*).

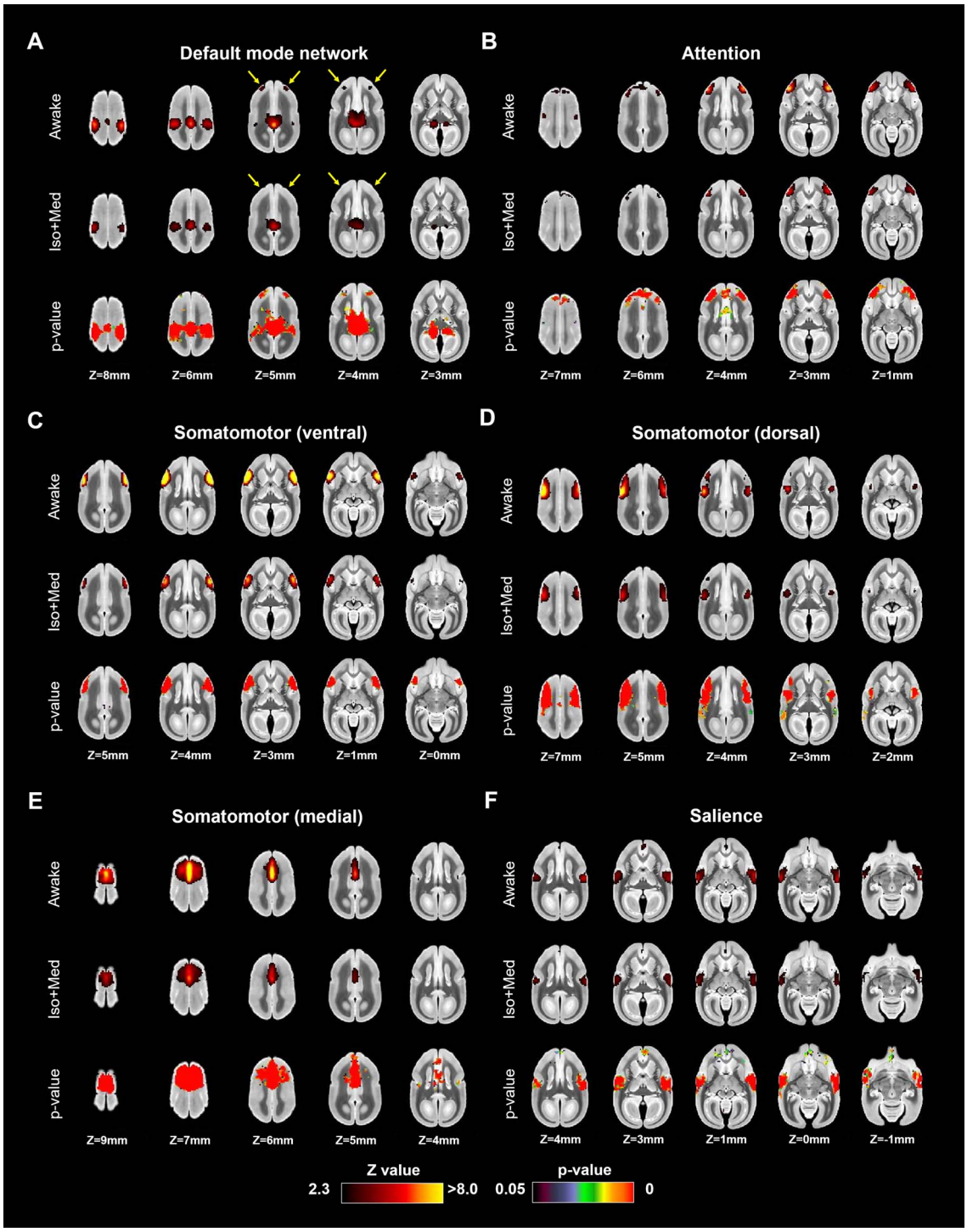

Figure 2. Coactivation areas in marmosets under awake (first row) and isoflurane with medical air (Iso + Med) conditions (second row) for (*A*) default mode, (*B*) attention, (*C*) somatomotor (ventral), (*D*) somatomotor (dorsal), (*E*) somatomotor (medial), and (*F*) salience networks (other four in Figure 3). The bottom rows in each component indicate *P*-value images, showing statistically lower activation areas in the anesthetized condition than in the awake condition. Yellow arrows indicate the differences of lateral frontal cortex activations in default mode network.

The Effects of Isoflurane on Thalamic Connectivity

The FC maps from left thalamus are shown in lateral-medial (Fig. 7*A* and *B*) and dorsal-ventral views (Fig. 7*C* and *D*) for cortex, and in volume view for subcortical areas (Fig. 7*E* and *F*). The thalamic VOI are presented in Figure 7*I*. The thalamus in awake marmosets was highly connected to frontal areas (A8aV, A8b, A9, A11, A13M, A32, A45, A47L), temporal areas (AuA1, AuCL, AuML, AuR, FST, MST, PGa-IPa, V4T, V5), occipital areas (V1), cerebellum, and contralateral thalamus. In addition, the thalamus was negatively connected to parietal areas (PE, PF, PFG)

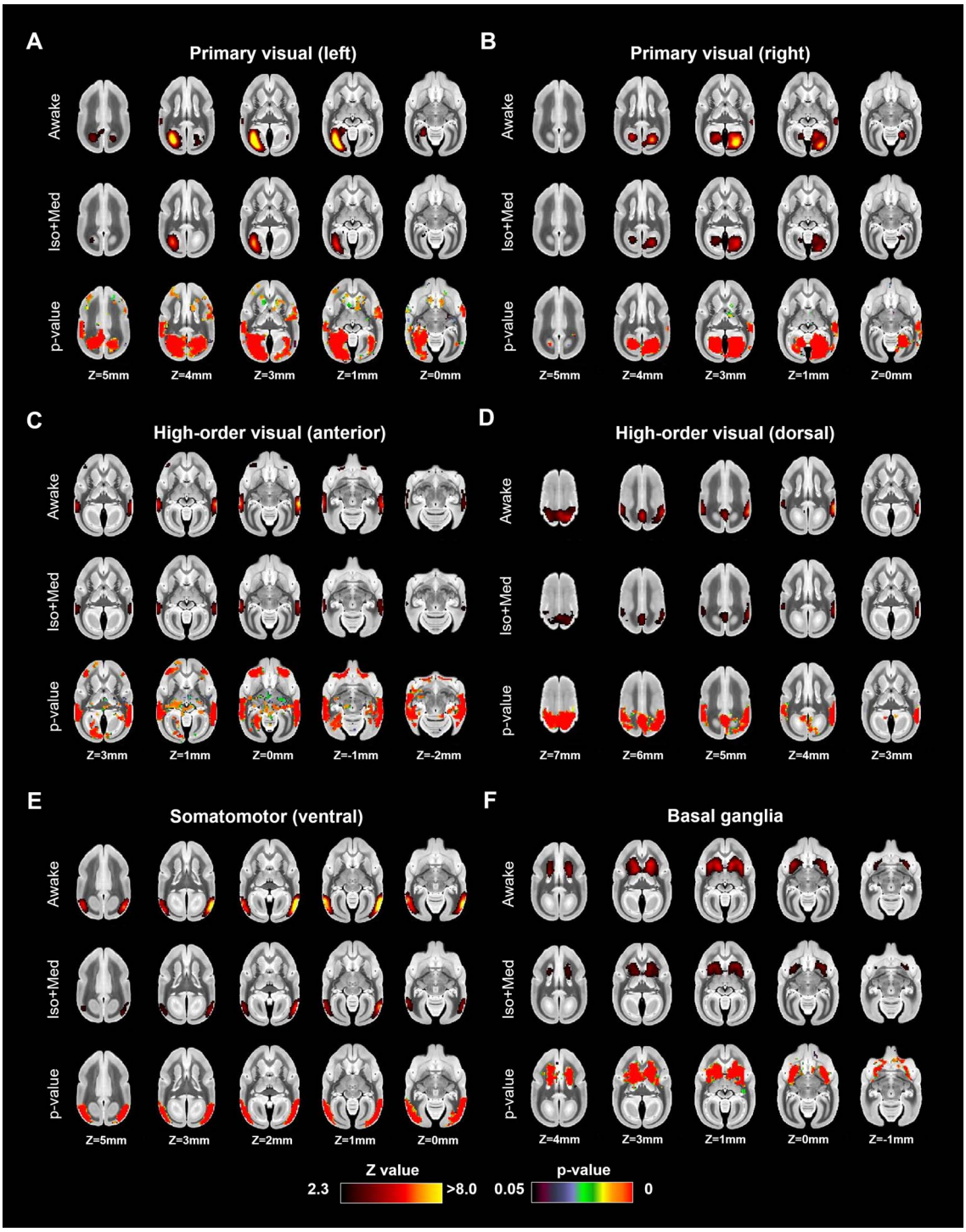

Figure 3. Coactivation areas in marmosets under awake (first row) and isoflurane with medical air (Iso + Med) conditions (second row) for (*A*) left primary visual, (*B*) right primary visual, (*C*) high-order visual (anterior), (*D*) high-order visual (dorsal), (*E*) high-order visual (ventral), and (*F*) basal ganglia networks (other four in Fig. 2). The bottom rows in each component indicate *P*-value images, showing statistically lower activation areas in the anesthetized condition than in the awake condition.

and posterior cingulate cortex (A23a, A23b, A31). However, the FC of these regions was drastically reduced by anesthesia. This finding was similar for the right thalamus. The regression line between thalamic connections under awake and Iso + Med was expressed as $CC(Iso + Med) = 0.30 \times CC(Awake) + 0.083$, while the regression line for whole brain regions was expressed as $CC(Iso + Med) = 0.44 \times CC(Awake) + 0.070$ (Fig. 7G). Overall, these results suggest that thalamic FC is more affected by isoflurane than other connections. Most of thalamic connections under anesthesia were within −0.5 to 0.5, while there were some

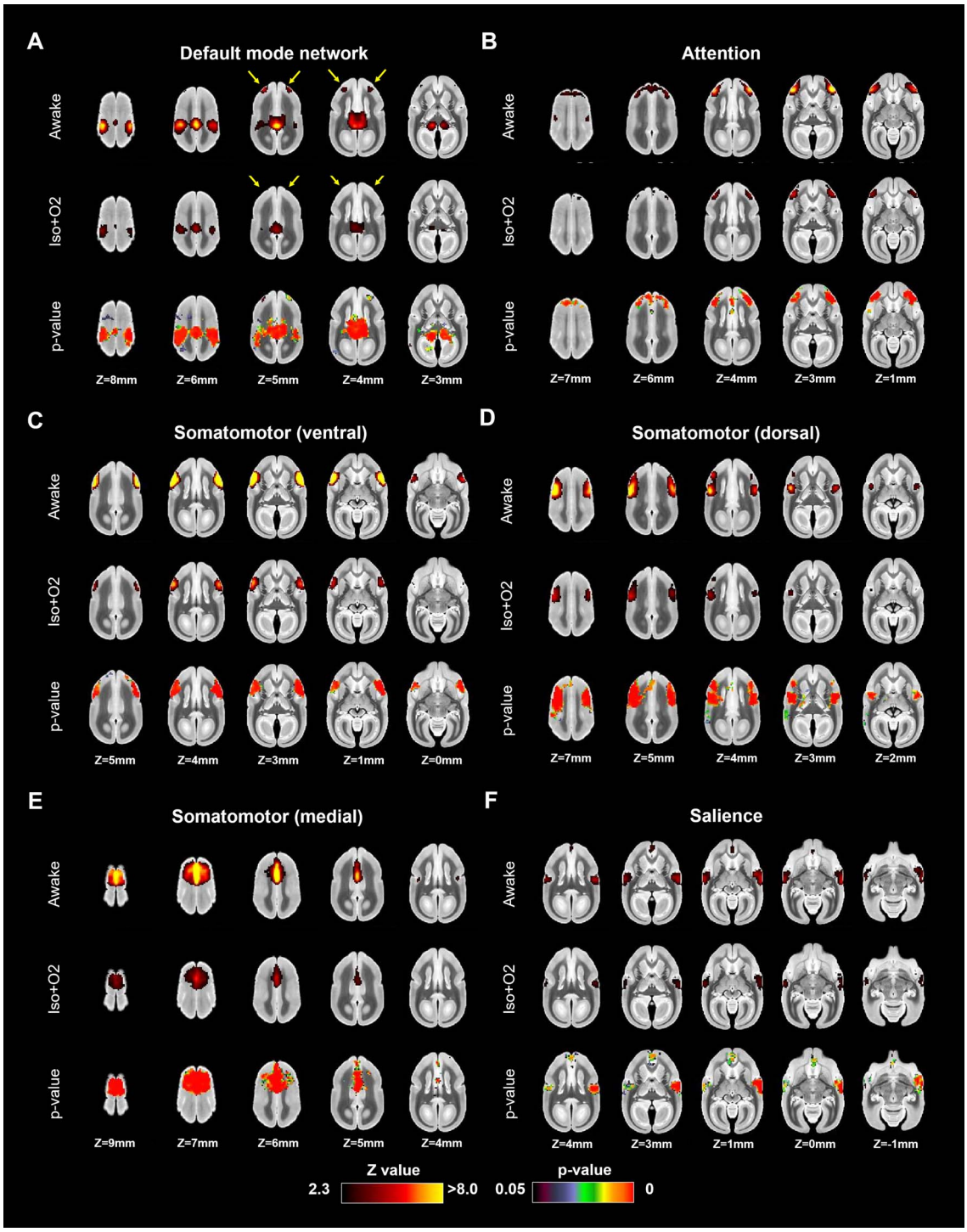

Figure 4. Coactivation areas in marmosets under awake (first row) and isoflurane with 100% oxygen (Iso + O_2) conditions (second row) for (*A*) default mode, (*B*) attention, (*C*) somatomotor (ventral), (*D*) somatomotor (dorsal), (*E*) somatomotor (medial), and (*F*) salience networks (other four in Fig. 5). The bottom rows in each component indicate *P*-value images, showing statistically lower activation areas in the anesthetized condition than in the awake condition. Yellow arrows indicate the differences of lateral frontal cortex activations in default mode network.

thalamic connections with correlation coefficients of over 0.5 under awake conditions (Fig. 7*H*). Paired-sample *t*-tests showed differences between awake and anesthetized FC from thalamus in orbitofrontal cortex (A11, A13M), MT, V1, contralateral thalamus, and cerebellum (Fig. 8).

Discussion

In this study, we investigated the effects of isoflurane, a commonly used inhalant anesthesia for nonhuman primate MRI, on the organization of functional resting-state networks in

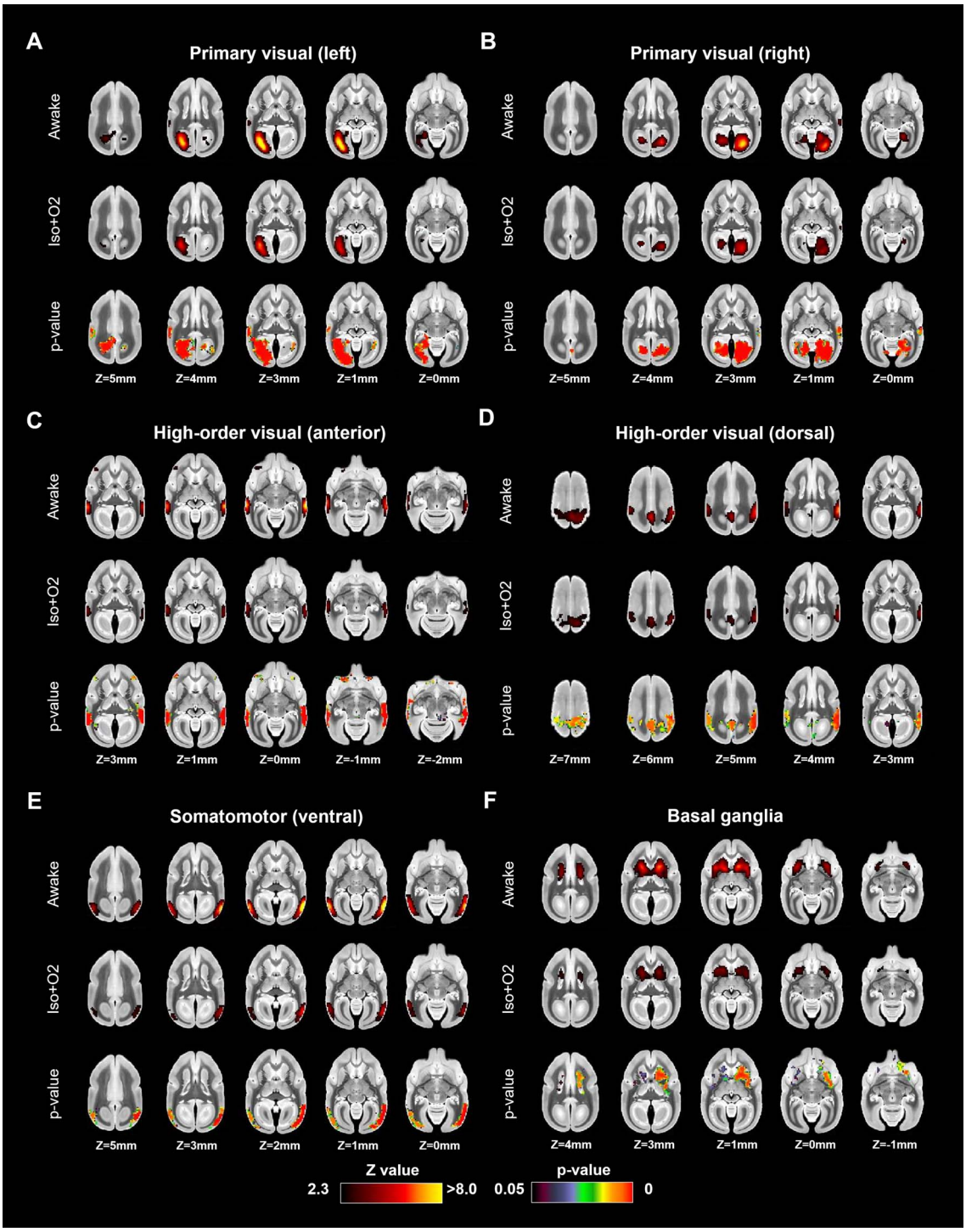

Figure 5. Coactivation areas in marmosets under awake (first row) and isoflurane with 100% oxygen ($Iso + O_2$) conditions (second row) for (*A*) left primary visual, (*B*) right primary visual, (*C*) high-order visual (anterior), (*D*) high-order visual (dorsal), (*E*) high-order visual (ventral), and (*F*) basal ganglia networks (other four in Fig. 4). The bottom rows in each component indicate *P*-value images, showing statistically lower activation areas in the anesthetized condition than in the awake condition.

marmosets. First, we derived functional networks from RS-fMRI data acquired in fully awake marmosets breathing room air, then compared the strength and structure of these networks to data in the same animals acquired under isoflurane anesthesia. To disentangle the potentially interactive effects of breathing gas delivery during the anesthetized scans, we collected data with either with medical air (21% oxygen) or 100% oxygen. Generally, although isoflurane globally decreased FC in resting-state networks, the spatial structure of the networks was preserved—this was the case for both medical air and

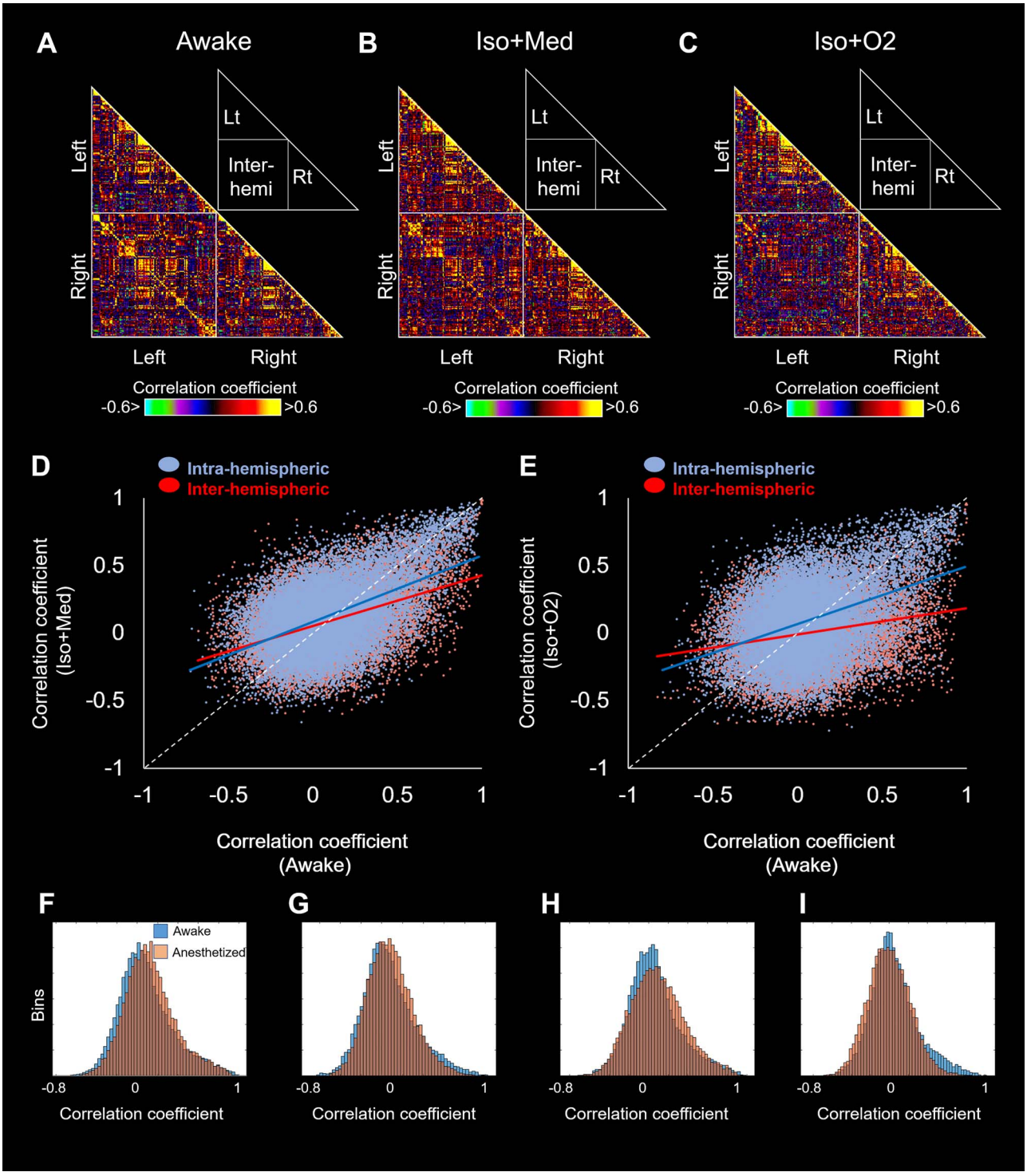

Figure 6. Correlation matrices among volume-of-interests (VOIs) for awake (*A*), Iso + Med (*B*), and Iso + O_2 (*C*) conditions. The relationship of correlation coefficients between awake and Iso + Med conditions (*D*), between awake and Iso + O_2 conditions (*E*). Blue and red circles indicate the plots for intra- and inter-hemispheric correlations, respectively. Each regression lines are also shown in the same color as each plot. The distributions of the correlation coefficients between awake and Iso + Med (*F*: intra-hemispheric; *G*: inter-hemispheric), and during awake and Iso + O_2 (*H*: intra-hemispheric; *I*: inter-hemispheric). Blue and orange bins indicate awake and anesthetized correlation coefficients, respectively.

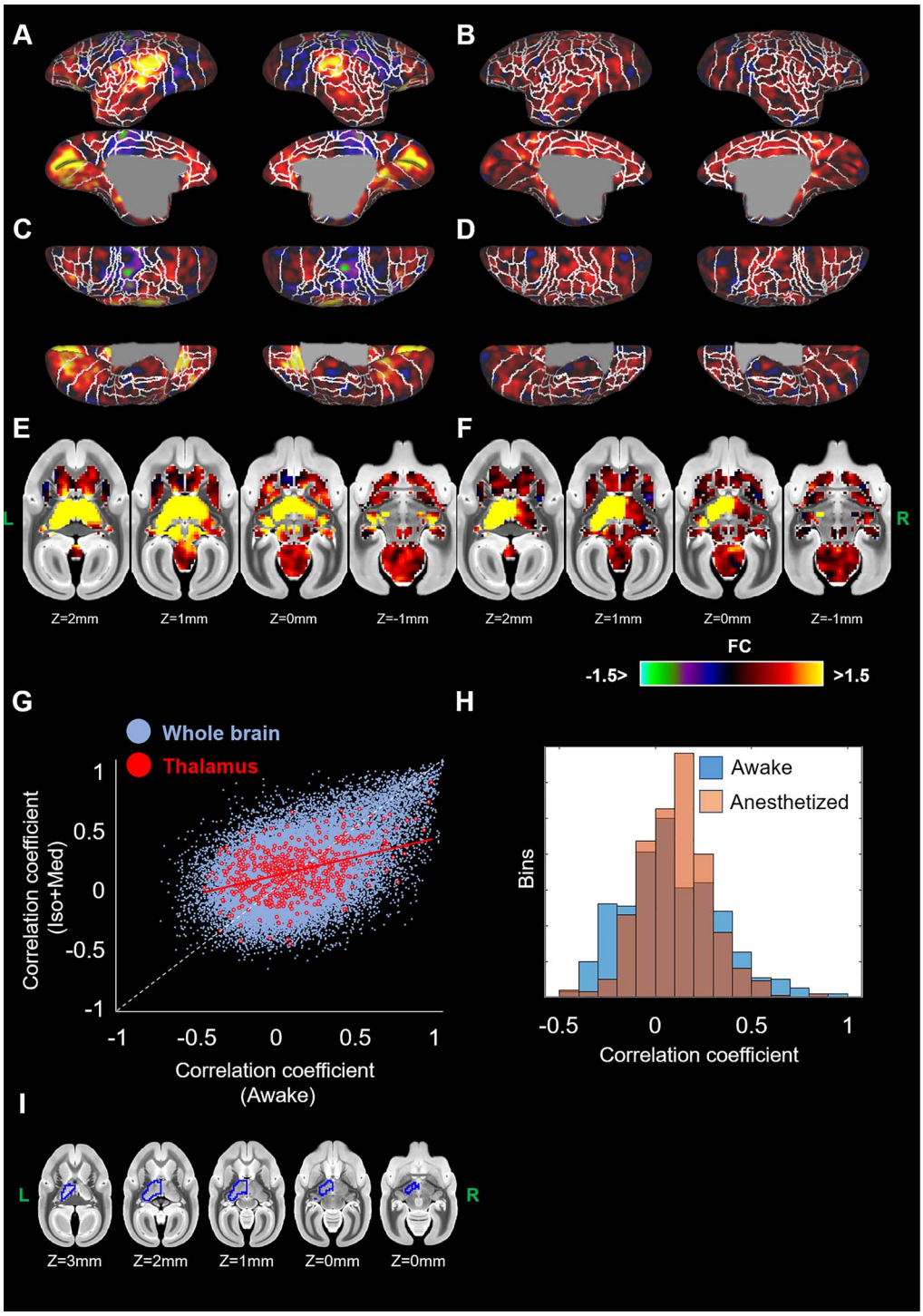

Figure 7. Seed-based functional connectivities (FCs) from left thalamus for awake (*A*, *C*, *E*) and anesthetized marmosets (*B*, *D*, *F*). Cortical maps are displayed on the surfaces in lateral-medial (*A*, *B*), and dorsal-ventral (*C*, *D*) views. Subcortical maps are shown in volume views (*E*, *F*). (*G*) The relationship of thalamic connections between awake and Iso + Med conditions. Blue and red circles indicate the connections among whole brain regions (same plots in Fig. 6D) and those with thalamus, respectively. (*H*) The distributions of the thalamic connections (correlation coefficients) of awake (blue) and anesthesia (orange). (*I*) Red lines indicate regression line for thalamic connections. The seed region (left thalamus) was indicated by blue line.

100% oxygen. Outside of the context of RS networks, we indexed pair-wise functional connectivity between regions across the brain and found that isoflurane substantially altered interhemispheric and thalamic FC.

Awake Resting-state Functional Networks

To isolate resting state networks across the brain, we applied an independent component analysis (Smith et al. 2004) to the RS-fMRI data acquired while the marmosets were fully

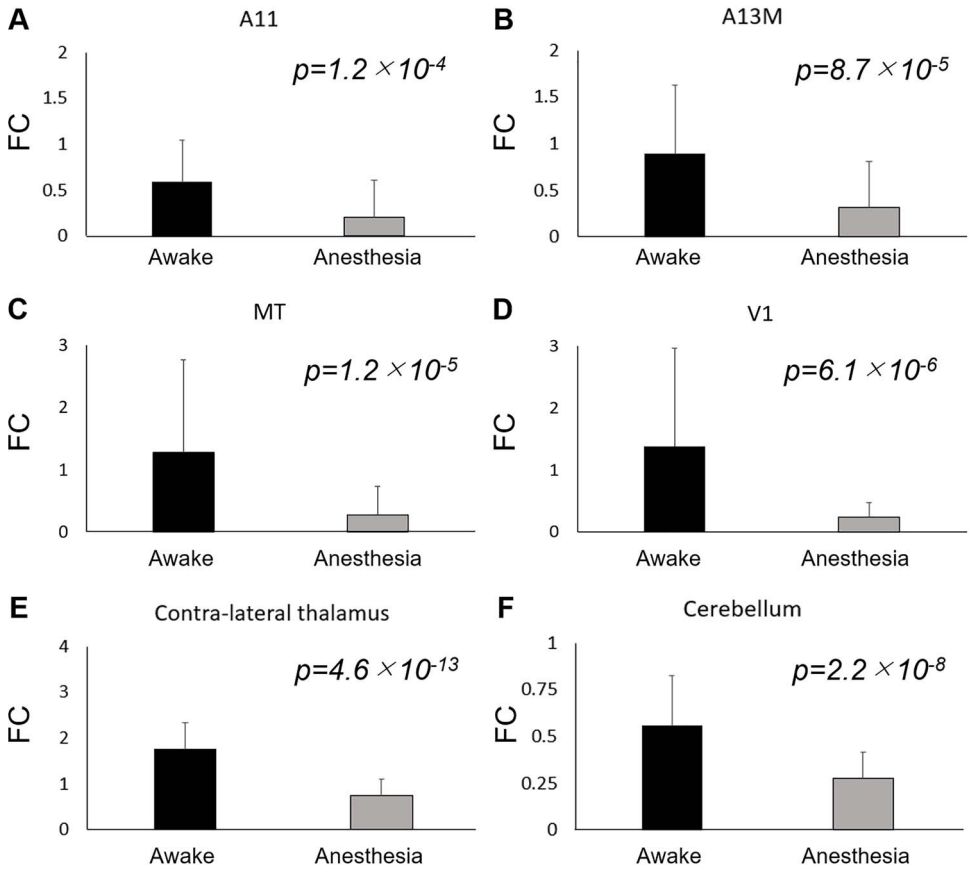

Figure 8. Strength of functional connectivity (FC) from thalamus in awake and anesthetized (Iso + Med) marmosets. The FCs in A11 (*A*), A13M (*B*), MT (*C*), V1 (*D*), contra-lateral thalamus (*E*), and cerebellum (*F*) show statistically significant differences between awake and anesthetized monkeys. The error bars indicate standard deviations among scans.

awake—these networks were then used as spatial templates to compare to the anesthetized data using a dual regression technique (Filippini et al. 2009). With this analysis, we obtained 12 RSNs, including a default mode network, an attention network, three somatomotor networks, a salience network, five visual-related networks, and a basal ganglia network. All 12 of these networks demonstrated clear bilateral correlation patterns, with the exception of the primary visual network, which were identified in separate left and right components (see Fig. 1). These networks were generally convergent with patterns identified by a previous report in awake marmosets (Belcher et al. 2013; Liu et al. 2019), albeit we could not detect the cerebellar, the orbitofrontal, and frontal pole RSNs—we suspect that these differences may be the result of suboptimal signal to noise ratios (SNR) in these areas due to the design of our coil (Fig. 9). Indeed, the spatial correlations in the orbitofrontal and the frontal pole networks across the sessions were relatively low in the aforementioned report (Belcher et al. 2013). The SNR profile of our coil may also account for the additional attention and dorsal somatomotor RSNs we observed with our data—unlike cerebellum, these networks resided in areas in which our SNR was highest, which may have given us more power to detect these networks at 9.4 Tesla (previous reports at 7 Tesla; Belcher et al. 2013). Overall, however, our data corroborates the majority of the RS networks previously identified in marmosets (Belcher et al. 2013; Liu et al. 2019).

Effects of Isoflurane on Functional Networks

Using dual regression, we compared the 12 ICA-derived networks between the awake and anesthesia conditions, with the awake networks serving as the baseline comparator. Generally, we found that isoflurane decreased coactivations in all cortical networks, and this was the case with both medical air and 100% oxygen. This is consistent with data from macaques, wherein isoflurane reduced the cortical coactivations in fronto-parietal, frontal, posterior-parietal, superior-temporal, and precentral-temporal networks (Hutchison et al. 2014). Although FC was reduced by isoflurane, the general structure of the networks was preserved at an isoflurane level of 1.5%. The default mode network seemed to be disproportionally affected by the reduction in FC, to the extent that the frontal component of this network was not present (i.e., subthreshold) when the animals were anesthetized. As shown in a previous DMN study in marmosets, for example, connections between frontal cortex and posterior parietal cortex (PPC) are relatively low (0.42–0.47) compared to PPC with PCC (e.g., PPC-PCC 0.65–0.70) (Liu et al. 2019). Our work also showed that frontal activation was lower than in other DMN regions (PPC, PCC). Thus, the frontal component of this network was not presented (i.e., was below statistical). Therefore, isoflurane anesthesia may obfuscate the full extent of this network in marmosets. This tendency was similar to a previous human study that showed that local connectivity of frontal cortex in the default mode network was dramatically reduced by

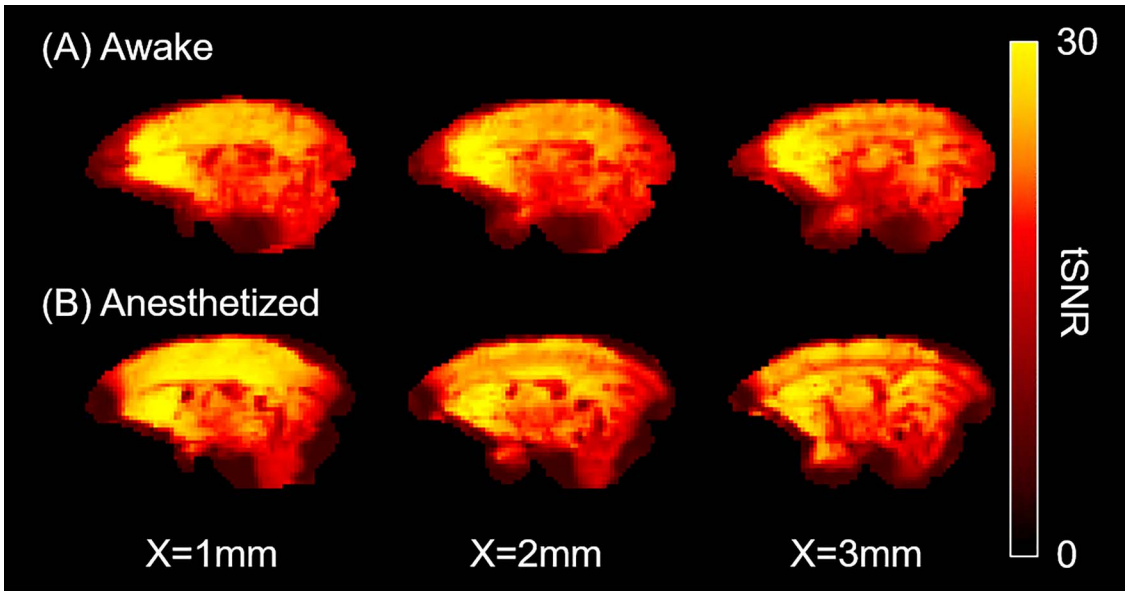

Figure 9. Representative temporal signal-to-noise (tSNR) maps of awake (*A*) and anesthetized marmosets (*B*). The tSNR were lower in frontal pole and cerebellum than in other regions, but the tSNR were similarly distributed across two conditions.

1% sevoflurane anesthesia even though other patterns (anterior and posterior cingulate cortex, inferior parietal cortex) were detected (Deshpande et al. 2010). Accordingly, if collection of awake RS-fMRI is not possible, then a lower isoflurane concentration, perhaps in combination with other anesthetics (e.g., medetomidine), may be better suited for studying the marmoset default mode network or specific functional connectivity under anesthesia (Grandjean et al. 2014).

Comparison of Functional Networks Between Awake State and Iso + O_2 Conditions

In marmosets, RS-fMRI is often performed under isoflurane anesthesia in combination with high-concentration oxygen (Sadagopan et al. 2015; Ghahremani et al. 2016; Schaeffer, Gilbert, Gati, et al. 2019a; Schaeffer, Gilbert, Ghahremani, et al. 2019b; Hori et al. 2020). As such, these studies are altering both the amount of anesthesia and the amount of oxygen that the marmoset is receiving—here, we sought to test the effect of using 100% oxygen versus medical air, which has the same oxygen level as room air (21%). Simply put, we did not find differences between these two conditions, suggesting that the effects of the inhalant anesthesia were due to the isoflurane, rather than the oxygen concentration. Although previous studies showed that BOLD signal was temporally corrected with changes in oxygen partial pressure (Karczmar et al. 1994; Baudelet and Gallez 2002), the effects of 1.5% isoflurane on functional connectivity might be larger than those of oxygen concentration. These findings suggest the validity of the conventional protocol (Iso + O_2) to measure the overall structure of the functional networks. Using this protocol, for example, our group has revealed the functional boundaries in anterior cingulate cortex and lateral prefrontal cortex in marmosets (Schaeffer, Gilbert, Gati, et al. 2019a; Schaeffer, Gilbert, Ghahremani, et al. 2019b) and functional connectivity patterns of the saccadic eye movement network (Ghahremani et al. 2016).

Effects of Isoflurane on Thalamic Connectivity

There is clear evidence that anesthetics affect brain activation in the thalamus (Miller and Ferrendelli 1990; Detsch et al. 1999; Alkire et al. 2007, 2008). To examine the effects of isoflurane on thalamic connectivity, we performed seed-based analyses. In awake marmosets, a large seed in the thalamus, including anterior part, laterodorsal, mediodorsal, ventral anterior, ventral lateral, ventral posterior thalamic nuclei, and pulvinar was functionally connected to frontal (A8aV, A8b, A9, A11, A13M, A32, A45, A47L), temporal (AuA1, AuCL, AuML, AuR, FST, MST, PGa-IPa, V4T, V5), and visual areas (V1, V2, V3), cerebellum, and contralateral thalamus. We also found negative thalamic correlations with parietal areas and posterior cingulate cortex. This tendency was similar to the previous human studies that showed negative thalamo-cortical correlations (Zhang et al. 2008; Zou et al. 2009; Chen et al. 2019). Although the FC obtained by RS-fMRI simply refers to the correlation of BOLD signals across time between two regions, the invasive nonhuman primate studies demonstrate the fluctuation of BOLD signal has a neurophysiological origin (Logothetis et al. 2001; Schölvinck et al. 2010). Indeed, RS-fMRI allows for the evaluation of functional network/connectivity changes as a function of various neuropathologies (for a review see Greicius 2008). However, it is still unclear what negative correlations mean. Note that, given that thalamic connectivity was disproportionally and drastically reduced by isoflurane, studies interested in thalamic connectivity should avoid the use of isoflurane.

We also observed significant differences between awake and anesthetized monkeys in orbitofrontal regions (A11, A13M), V1, MT, cerebellum, and contralateral thalamic connections. It is known that anesthetic effects on the thalamus may be indirect (Schiff and Plum 2000; Vahle-Hinz et al. 2007; Franks 2008), as spontaneous thalamic firing during anesthesia is largely caused by feedback from cortical neurons (Vahle-Hinz et al. 2007), especially anesthetic-sensitive layer V cells (Angel 1993; Laureys 2006). Other findings show that thalamocortical neurons reduce their activity for isoflurane concentration

higher than 1.0% (Detsch et al. 1999). Cortico-thalamo-cortical functional disconnections are observed in vegetative patients, and miracle recovery from this state may be caused by the restoration of FC between thalamus and cortex (Laureys, 2006). Recently, it has been shown that microstimulation of the central thalamus in anesthetized macaques restores arousal and wake-like neural activity in cortex (Redinbaugh et al. 2020). In addition, two-photon calcium imaging in mice and micro-electrode array recordings in humans have provided evidence to suggest that functional connectivity of the cortex breaks down at the microlevel depending on the level of medically induced loss of consciousness (mLOC) (Wenzel et al. 2019). Therefore, the attenuated FC between cortex and thalamus might reflect a neural mechanism for isoflurane-induced anesthesia.

Comparison of Previous Macaque Findings

The effects of anesthesia on FC in non-human primates has already been well studied in macaque monkeys (Vincent et al. 2007; Hutchison et al. 2014; Barttfeld et al. 2015; Uhrig et al. 2018). Our group has previously shown that the effects of isoflurane are larger for interhemispheric connections than for intra-hemispheric connections (Hutchison et al. 2014). Barttfeld and his colleagues have elucidated the reductions of negative correlations by anesthesia (Barttfeld et al. 2015) and have suggested that the presence of negative correlations is a characteristic of wakefulness. These findings were consistent with our results that 1) anesthesia (Iso + Med) induced substantially reductions of strong interhemispheric connections (Fig. 6G), but intra-hemispheric connections were preserved (Fig. 6F); 2) the peak of the distribution of connections (correlation coefficients) was shifted in the positive direction by isoflurane for both intra- and interhemispheric connections (Fig. 6F and G), so that negative correlations were decreased. Although the nature of such negative correlations has been debated (possibilities of artifacts such as temporal filtering and subtraction of the mean brain activity), our findings suggest that functional configuration by anesthesia is preserved between macaques and marmosets.

Considerations

In this study, anesthesia was induced using intramuscular injection of ketamine around 30 min before starting RS-fMRI scans under isoflurane anesthesia. Thus, RS-fMRI may have been affected by not only isoflurane, but also ketamine. However, we could not find any differences between first (30 min from ketamine injection) and last runs (80–90 min from ketamine injection). Given the typical timeline of the behavioral effects of intramuscular injections of ketamine (Holcomb et al. 2005; Skoblenick and Everling 2012), a strong effect of ketamine would likely be more apparent soon after the injection, but less so 90 min after the injection. This was not the case here, with no differences in FC between the first and last runs.

Here, we used 1.5% isoflurane anesthesia to elucidate the effects on functional network connectivity in marmosets, because this concentration is commonly used for RS-fMRI studies in non-human primates (Milham et al. 2020). While dose-dependency is a very important question, our aim was to quantify the changes based on canonical dosing for RS-fMRI studies in nonhuman primates (Hutchison et al. 2011, 2014; Sadagopan et al. 2015; Ghahremani et al. 2016; Schaeffer, Gilbert, Gati, et al. 2019a; Schaeffer, Gilbert, Ghahremani, et al. 2019b; Hori et al. 2020).

We showed a clear reduction in lateral frontal cortex in the default mode network as well as in thalamic and interhemispheric connections under isoflurane anesthesia. It is possible that the use of other anesthetic agents or a combination of different agents might be able to avoid or reduce these suppressive effects on FC. For example, Grandjean et al. (2014) compared the effects of four commonly used anesthetics (isoflurane, propofol, urethane, and medetomidine) on RS-fMRI in mice. They showed that bilateral striatal FC was detected under medetomidine anesthesia, but not under isoflurane, propofol, or urethane anesthesia. They also showed that a combination of low-dose medetomidine and isoflurane offer strong correlations both within cortical and subcortical structures without potential seizure-inducing effects. It remains to be tested whether an anesthesia protocol involving medetomidine and isoflurane might be better suited to also preserve the default mode network and corticothalamic connections in marmosets.

Another caveat of using RS-fMRI to study the effect of anesthesia is that canonically derived FC between two brain areas simply refers to the correlation of blood oxygen level-dependent (BOLD) signals across time (i.e., with no information about the underlying axons and synapses responsible for connections); thus, it is an indirect method to measure the neural connections. Additionally, there are some potential confounds that could affect BOLD signals or FC, such as end-tidal CO_2 (Et-CO_2) fluctuations, eye movements, CSF pulsation, and heart rate. In an effort to account for these confounding variables, we did apply an ICA-based denoising technique to remove the structured noise, but some of these variables, such as Et-CO_2, are more difficult to remove with this method, given that the frequency is similar to that of BOLD signals being measured (Wise et al. 2004)—some studies have shown that small fluctuations in Et-CO_2 occur naturally during normal breathing at rest and are significantly correlated with BOLD fMRI signal fluctuations (Wise et al. 2004). As such, measuring Et-CO_2 directly would be more ideal from a modeling perspective, but is difficult to measure in fully awake marmosets. That being said, it is unlikely that such variables had a profound effect on the present results—indeed, our group quantitatively evaluated the relationship between FC obtained by RS-fMRI under isoflurane anesthesia and tracer-based directional connectivity, namely monosynaptic axonal pathways (Hori et al. 2020). These results showed that overall FC was highly correlated with tracer-based connectivity, supporting the feasibility of FC to infer how strongly different brain areas are connected *in vivo*.

Conclusion

Overall, our findings indicate that RS-fMRI under isoflurane anesthesia is useful to evaluate the global structure of functional networks in marmosets, but RS-fMRI under in awake animals may be required to identify the full extent of the default mode network as well as pairwise regional connectivity, particularly for thalamic and interhemispheric connections. Furthermore, we observed that the effects of anesthesia on network connectivity showed very little differences when delivered with medical air or with 100% oxygen.

Author Contributions

Y.H., D.J.S. and S.E. designed research; Y.H., D.J.S., K.M.G., L.K.H., J.C.C., J.S.G. and S.E. performed research; Y.H. and D.J.S. analyzed

data; Y.H. and D.J.S. wrote the paper; and Y.H., D.J.S., K.M.G., L.K.H., J.C.C., J.S.G., R.S.M. and S.E. edited the paper.

Funding

Canadian Institutes of Health Research (grants FRN 148365, FRN 353372); Canada First Research Excellence Fund to BrainsCAN.

Notes

We thank Miranda Bellyou for animal preparation and care and Dr Alex Li for scanning assistance. *Conflict of Interest*: None declared.

References

Alkire MT, Hudetz AG, Tononi G. 2008. Consciousness and anesthesia. *Science*. 322:876–880. doi: 10.1126/science.1149213.

Alkire MT, McReynolds JR, Hahn EL, Trivedi AN. 2007. Thalamic microinjection of nicotine reverses sevoflurane-induced loss of righting reflex in the rat. *Anesthesiology*. 107:264–272. doi: 10.1097/01.anes.0000270741.33766.24.

Angel A. 1993. Central neuronal pathways and the process of anaesthesia. *Br J Anaesth*. 71:148–163. doi: 10.1093/bja/71.1.148.

Barttfeld P, Uhrig L, Sitt JD, Sigman M, Jarraya B, Dehaene S. 2015. Signature of consciousness in the dynamics of resting-state brain activity. *Proc Natl Acad Sci U S A*. 112:887–892. doi: 10.1073/pnas.1418031112.

Baudelet C, Gallez B. 2002. How does blood oxygen level-dependent (BOLD) contrast correlate with oxygen partial pressure (pO_2) inside tumors? *Magn Reson Med*. 48:980–986. doi: 10.1002/mrm.10318.

Belcher AM, Yen CC, Stepp H, Gu H, Lu H, Yang Y, Silva AC, Stein EA. 2013. Large-scale brain networks in the awake, truly resting marmoset monkey. *J Neurosci*. 33:16796–16804. doi: 10.1523/JNEUROSCI.3146-13.2013.

Belcher AM, Yen CCC, Notardonato L, Ross TJ, Volkow ND, Yang Y, Stein EA, Silva AC, Tomasi D. 2016. Functional connectivity hubs and networks in the awake marmoset brain. *Front. Integr. Neurosci*. 10:9. doi: 10.3389/fnint.2016.00009.

Boveroux P, Vanhaudenhuyse A, Bruno MA, Noirhomme Q, Lauwick S, Luxen A, Degueldre C, Plenevaux A, Schnakers C, Phillips C *et al*. 2010. Breakdown of within- and between-network resting state functional magnetic resonance imaging connectivity during propofol-induced loss of consciousness. *Anesthesiology*. 113:1038–1053. doi: 10.1097/ALN.0b013e3181f697f5.

Buxton RB. 2010. Interpreting oxygenation-based neuroimaging signals: the importance and the challenge of understanding brain oxygen metabolism. *Front Neuroenerg*. 2:8. doi: 10.3389/fnene.2010.00008.

Chen P, Ye E, Jin X, Zhu Y, Wang L. 2019. Association between thalamocortical functional connectivity abnormalities and cognitive deficits in schizophrenia. *Sci Rep*. 9:2952. doi: 10.1038/s41598-019-39367-z.

Deshpande G, Kerssens C, Sebel PS, Hu X. 2010. Altered local coherence in the default mode network due to sevoflurane anesthesia. *Brain Res*. 1318:110–121. doi: 10.1016/j.brainres.2009.12.075.

Detsch O, Vahle-Hinz C, Kochs E, Siemers M, Bromm B. 1999. Isoflurane induces dose-dependent changes of thalamic somatosensory information transfer. *Brain Res*. 829:77–89. doi: 10.1016/S0006-8993(99)01341-4.

Ebina T, Masamizu Y, Tanaka YR, Watakabe A, Hirakawa R, Hirayama Y, Hira R, Terada SI, Koketsu D, Hikosaka K *et al*. 2018. Two-photon imaging of neuronal activity in motor cortex of marmosets during upper-limb movement tasks. *Nat. Commun*. 9:1879. doi: 10.1038/s41467-018-04286-6.

Filippini N, MacIntosh BJ, Hough MG, Goodwin GM, Frisoni GB, Smith SM, Matthews PM, Beckmann CF, Mackay CE. 2009. Distinct patterns of brain activity in young carriers of the APOE-4 allele. *Proc Natl Acad Sci U S A*. 106:7209–7214. doi: 10.1073/pnas.0811879106.

Franks NP. 2008. General anaesthesia: from molecular targets to neuronal pathways of sleep and arousal. *Nat Rev Neurosci*. 9:370–386. doi: 10.1038/nrn2372.

Gagnon L, Sakadzic S, Lesage F, Musacchia JJ, Lefebvre J, Fang Q, Yucel MA, Evans KC, Mandeville ET, Cohen-Adad J *et al*. 2015. Quantifying the microvascular origin of BOLD-fMRI from first principles with two-photon microscopy and an oxygen-sensitive nanoprobe. *J Neurosci*. 35:3663–3675. doi: 10.1523/JNEUROSCI.3555-14.2015.

Ghahremani M, Hutchison RM, Menon RS, Everling S. 2016. Frontoparietal functional connectivity in the common marmoset. *Cereb Cortex*. 27:3890–3905. doi: 10.1093/cercor/bhw198.

Grandjean J, Schroeter A, Batata I, Rudin M. 2014. Optimization of anesthesia protocol for resting-state fMRI in mice based on differential effects of anesthetics on functional connectivity patterns. *Neuroimage*. 102:838–847. doi: 10.1016/j.neuroimage.2014.08.043.

Greicius MD. 2008. Resting-state functional connectivity in neuropsychiatric disorders. *Curr Opin Neurol*. 24:424–430. doi: 10.1097/WCO.0b013e328306f2c5.

Greicius MD, Kiviniemi V, Tervonen O, Vainionpää V, Alahuhta S, Reiss AL, Menon V. 2008. Persistent default-mode network connectivity during light sedation. *Hum Brain Mapp*. 29:839–847. doi: 10.1002/hbm.20537.

Griffanti L, Douaud G, Bijsterbosch J, Evangelisti S, Alfaro-Almagro F, Glasser MF, Duff EP, Fitzgibbon S, Westphal R, Carone D *et al*. 2017. Hand classification of fMRI ICA noise components. *Neuroimage*. 154:188–205. doi: 10.1016/j.neuroimage.2016.12.036.

Hashikawa T, Nakatomi R, Iriki A. 2015. Current models of the marmoset brain. *Neurosci Res*. 93:116–127. doi: 10.1016/j.neures.2015.01.009.

Holcomb HH, Lahti AC, Medoff DR, Cullen T, Tamminga CA. 2005. Effects of noncompetitive NMDA receptor blockade on anterior cingulate cerebral blood flow in volunteers with schizophrenia. *Neuropsychopharmacology*. 30:2275–2282. doi: 10.1038/sj.npp.130082.

Hori Y, Schaeffer DJ, Gilbert KM, Hayrynen LK, Cléry JC, Gati JS, Menon RS, Everling S. 2020. Comparison of resting-state functional connectivity in marmosets with tracer-based cellular connectivity. *Neuroimage*. 204:116241. doi: 10.1016/j.neuroimage.2019.116241.

Hutchison RM, Hutchison M, Manning KY, Menon RS, Everling S. 2014. Isoflurane induces dose-dependent alterations in the cortical connectivity profiles and dynamic properties of the brain's functional architecture: dose-dependent Isoflurane effects. *Hum Brain Mapp*. 35:5754–5775. doi: 10.1002/hbm.22583.

Hutchison RM, Leung LS, Mirsattari SM, Gati JS, Menon RS, Everling S. 2011. Resting-state networks in the macaque

at 7T. *Neuroimage*. 56:1546–1555. doi: 10.1016/j.neuroimage.2011.02.063.

Johnston KD, Barker K, Schaeffer L, Schaeffer DJ, Everling S. 2018. Methods for chair restraint and training of the common marmoset on oculomotor tasks. *J. Neurophysiol*. 119:1636–1646. doi: 10.1152/jn.00866.2017.

Johnston K, Ma L, Schaeffer L, Everling S. 2019. Alpha-oscillations modulate preparatory activity in marmoset area 8Ad. *J. Neurosci*. 39:2703–2718. doi: 10.1523/JNEUROSCI.2703-18.2019.

Karczmar GS, River JN, Li J, Vijayakumar S, Goldman Z, Lewis MZ. 1994. Effects of hyperoxia on T∗2 and resonance frequency weighted magnetic resonance images of rodent tumours. *NMR Biomed*. 7:3–11. doi: 10.1002/nbm.1940070103.

Kondo T, Saito R, Otaka M, Yoshino-Saito K, Yamanaka A, Yamamori T, Watakabe A, Mizukami H, Schnitzer MJ, Tanaka KF *et al*. 2018. Calcium transient dynamics of neural ensembles in the primary motor cortex of naturally behaving monkeys. *Cell Rep*. 24:2191–2195.e4. doi: 10.1016/j.celrep.2018.07.057.

LaClair M, Febo M, Nephew B, Gervais NJ, Poirier G, Workman K, Chumachenko S, Payne L, Moore MC, King JA *et al*. 2019. Sex differences in cognitive flexibility and resting brain networks in middle-aged marmosets. *eNeuro*. 6:ENEURO.0154-19.2019. doi: 10.1523/ENEURO.0154-19.2019.

Laureys S. 2006. Tracking the recovery of consciousness from coma. *J Clin Investig*. 116:1823–1825. doi: 10.1172/JCI29172.

Li X, Morgan PS, Ashburner J, Smith J, Rorden C. 2016. The first step for neuroimaging data analysis: DICOM to NIfTI conversion. *J Neurosci Methods*. 264:47–56. doi: 10.1016/j.jneumeth.2016.03.001.

Liu C, Ye FQ, Yen CCC, Newman JD, Glen D, Leopold DA, Silva AC. 2018. A digital 3D atlas of the marmoset brain based on multi-modal MRI. *Neuroimage*. 169:106–116. doi: 10.1016/j.neuroimage.2017.12.004.

Liu C, Yen CCC, Szczupak D, Ye FQ, Leopold DA, Silva AC. 2019. Anatomical and functional investigation of the marmoset default mode network. *Nat Commun*. 10:1975. doi: 10.1038/s41467-019-09813-7.

Liu JV, Hirano Y, Nascimento GC, Stefanovic B, Leopold DA, Silva AC. 2013a. fMRI in the awake marmoset: somatosensory-evoked responses, functional connectivity, and comparison with propofol anesthesia. *Neuroimage*. 78:186–195. doi: 10.1016/j.neuroimage.2013.03.038.

Liu X, Pillay S, Li R, Vizuete JA, Pechman KR, Schmainda KM, Hudetz AG. 2013b. Multiphasic modification of intrinsic functional connectivity of the rat brain during increasing levels of propofol. *Neuroimage*. 83:581–592. doi: 10.1016/j.neuroimage.2013.07.003.

Liu X, Zhu XH, Zhang Y, Chen W. 2011. Neural origin of spontaneous hemodynamic fluctuations in rats under burst-suppression Anesthesia condition. *Cereb Cortex*. 21:374–384. doi: 10.1093/cercor/bhq105.

Logothetis NK, Pauls J, Augath M, Trinath T, Oeltermann A. 2001. Neurophysiological investigation of the basis of the fMRI signal. *Nature*. 412:150–157. https://www.nature.com/articles/35084005.

Marcus DS, Harwell J, Olsen T, Hodge M, Glasser MF, Prior F, Jenkinson M, Laumann T, Curtiss SW, Van Essen DC. 2011. Informatics and data mining tools and strategies for the human Connectome project. *Front. Neuroinform*. 5:4. doi: 10.3389/fninf.2011.00004.

Mars RB, Jbabdi S, Sallet J, O'Reilly JX, Croxson PL, Olivier E, Noonan MP, Bergmann C, Mitchell AS, Baxter MG *et al*. 2011. Diffusion-weighted imaging Tractography-based Parcellation of the human parietal cortex and comparison with human and macaque resting-state functional connectivity. *J Neurosci*. 31:4087–4100. doi: 10.1523/JNEUROSCI.5102-10.2011.

Martuzzi R, Ramani R, Qiu M, Rajeevan N, Constable RT. 2010. Functional connectivity and alterations in baseline brain state in humans. *Neuroimage*. 49:823–834. doi: 10.1016/j.neuroimage.2009.07.028.

Milham M, Petkov CI, Margulies DS, Schroeder CE, Basso MA, Belin P, Fair DA, Fox A, Kastner S, Mars RB *et al*. 2020. Accelerating the evolution of nonhuman primate neuroimaging. *Neuron*. 105:600–603. doi: 10.1016/j.neuron.2019.12.023.

Miller CT, Freiwald WA, Leopold DA, Mitchell JF, Silva AC, Wang X. 2016. Marmosets: a Neuroscientific model of human social behavior. *Neuron*. 90:219–233. doi: 10.1016/j.neuron.2016.03.018.

Miller JW, Ferrendelli JA. 1990. Characterization of gabaergic seizure regulation in the midline thalamus. *Neuropharmacology*. 29:649–655. doi: 10.1016/0028-3908(90)90026-N.

Mitchell JF, Leopold DA. 2015. The marmoset monkey as a model for visual neuroscience. *Neurosci Res*. 93:20–46. doi: 10.1016/j.neures.2015.01.008.

Ogawa S, Lee TM, Kay AR, Tank DW. 1990. Brain magnetic resonance imaging with contrast dependent on blood oxygenation. *Proc Natl Acad Sci U S A*. 87:9868–9872. doi: 10.1073/pnas.87.24.9868.

Okano H, Mitra P. 2015. Brain-mapping projects using the common marmoset. *Neurosci Res*. 93:3–7. doi: 10.1016/j.neures.2014.08.014.

Paasonen J, Stenroos P, Salo RA, Kiviniemi V, Gröh O. 2018. Functional connectivity under six anesthesia protocols and the awake condition in rat brain. *Neuroimage*. 172:9–20. doi: 10.1016/j.neuroimage.2018.01.014.

Park JE, Zhang XF, Choi SH, Okahara J, Sasaki E, Silva AC. 2016. Generation of transgenic marmosets expressing genetically encoded calcium indicators. *Sci Rep*. 6:34931. doi: 10.1038/srep34931.

Peltier SJ, Kerssens C, Hamann SB, Sebel PS, Byas-Smith M, Hu X. 2005. Functional connectivity changes with concentration of sevo£urane anesthesia. *Neuroreport*. 16:285–288.

Peterson, J., Chaddock, R., Dalrymple, B., Van Sas, F., Gilbert, K.M., Klassen, L.M., Gati, J.S., Handler, W.B., Chronik, B.A. 2018. Development of a gradient and shim insert system for marmoset imaging at 9.4 T. *Proceedings of the 26th Annual Meeting ISMRM*. Paris, France, p. 4421.

Redinbaugh MJ, Phillips JM, Kambi NA, Mohanta S, Andryk S, Dooley GL, Afrasiabi M, Raz A, Saalmann YB. 2020. Thalamus modulates consciousness via layer-specific control of cortex. *Neuron*[Epub ahead of print]. doi: 10.1016/j.neuron.2020.01.005.

Sadagopan S, Temiz-Karayol NZ, Voss HU. 2015. High-field functional magnetic resonance imaging of vocalization processing in marmosets. *Sci Rep*. 5:10950. doi: 10.1038/srep10950.

Sasaki E, Suemizu H, Shimada A, Hanazawa K, Oiwa R, Kamioka M, Tomioka I, Sotomaru Y, Hirakawa R, Eto T *et al*. 2009. Generation of transgenic non-human primates with germline transmission. *Nature*. 459:523–527. doi: 10.1038/nature08090.

Schaeffer DJ, Gilbert KM, Gati JS, Menon RS, Everling S. 2019a. Intrinsic functional boundaries of lateral frontal cortex in the common marmoset monkey. *J Neurosci*. 39:1020–1029. doi: 10.1523/JNEUROSCI.2595-18.2018.

Schaeffer DJ, Gilbert KM, Ghahremani M, Gati JS, Menon RS, Everling S. 2019b. Intrinsic functional clustering of anterior cingulate cortex in the common marmoset. *Neuroimage*. 186:301–307. doi: 10.1016/j.neuroimage.2018.11.005.

Schaeffer DJ, Gilbert KM, Hori Y, Gati JS, Menon RS, Everling S. 2019c. Integrated radiofrequency array and animal holder design for minimizing head motion during awake marmoset functional magnetic resonance imaging. *Neuroimage*. 193:126–138. doi: 10.1016/j.neuroimage.2019.03.023.

Schiff ND, Plum F. 2000. The role of arousal and "gating" Systems in the Neurology of impaired consciousness. *J Clin Neurophysiol*. 17:438–452. doi: 10.1097/00004691-200009000-00002.

Schölvinck ML, Maier A, Ye FQ, Duyn JH, Leopold DA. 2010. Neural basis of global resting-state fMRI activity. *Proc Natl Acad Sci U S A*. 107:10238–10243. doi: 10.1073/pnas.0913110107.

Shmuel A, Leopold DA. 2008. Neuronal correlates of spontaneous fluctuations in fMRI signals in monkey visual cortex: implications for functional connectivity at rest. *Hum Brain Mapp*. 29:751–761. doi: 10.1002/hbm.20580.

Silva AC, Liu JV, Hirano Y, Leoni RF, Merkle H, Mackel JB, Zhang XF, Nascimento GC, Stefanovic B. 2011. Longitudinal functional magnetic resonance imaging in animal models. *Methods Mol Biol*. 711:281–302.

Skoblenick K, Everling S. 2012. NMDA antagonist ketamine reduces task selectivity in macaque dorsolateral prefrontal neurons and impairs performance of randomly interleaved Prosaccades and Antisaccades. *J Neurosci*. 32:12018–12027. doi: 10.1523/JNEUROSCI.1510-12.2012.

Smith SM. 2002. Fast robust automated brain extraction. *Hum Brain Mapp*. 17:143–155. doi: 10.1002/hbm.10062.

Smith SM, Jenkinson M, Woolrich MW, Beckmann CF, Behrens TEJ, Johansen-Berg H, Bannister PR, De Luca M, Drobnjak I, Flitney DE *et al*. 2004. Advances in functional and structural MR image analysis and implementation as FSL. *Neuroimage*. 23:S208–S219. doi: 10.1016/j.neuroimage.2004.07.051.

T' Hart BA, Jagessar SA, Haanstra K, Verschoor E, Laman JD, Kap YS. 2013. The primate EAE model points at EBV-infected B cells as a preferential therapy target in multiple sclerosis. *Front. Immunol*. 4:145. doi: 10.3389/fimmu.2013.00145.

Tomioka I, Ishibashi H, Minakawa EN, Motohashi HH, Takayama O, Saito Y, Popiel HA, Puentes S, Owari K, Nakatani T *et al*. 2017. Transgenic monkey model of the Polyglutamine diseases recapitulating progressive neurological symptoms. *eNeuro*. 4:ENEURO.0250-16.2017. doi: 10.1523/ENEURO.0250-16.2017.

Tomioka I, Nogami N, Nakatani T, Owari K, Fujita N, Motohashi H, Takayama O, Takae K, Nagai Y, Seki K. 2017b. Generation of transgenic marmosets using a tetracyclin-inducible transgene expression system as a neurodegenerative disease model. *Biol Reprod*. 97:772–780. doi: 10.1093/biolre/iox129.

Uhrig L, Sitt JD, Jacob A, Tasserie J, Barttfeld P, Dupont M, Dehaene S, Jarraya B. 2018. Resting-state dynamics as a cortical signature of Anesthesia in monkeys. *Anesthesiology*. 129:942–958. doi: 10.1097/ALN.0000000000002336.

Vahle-Hinz C, Detsch O, Siemers M, Kochs E. 2007. Contributions of GABAergic and glutamatergic mechanisms to isoflurane-induced suppression of thalamic somatosensory information transfer. *Exp Brain Res*. 176:159–172. doi: 10.1007/s00221-006-0604-6.

Vincent JL, Patel GH, Fox MD, Snyder AZ, Baker JT, Van Essen DC, Zempel JM, Snyder LH, Corbetta M, Raichle ME. 2007. Intrinsic functional architecture in the anaesthetized monkey brain. *Nature*. 447:83–86. doi: 10.1038/nature05758.

Wegener S, Wong EC. 2008. Longitudinal MRI studies in the isoflurane-anesthetized rat: long-term effects of a short hypoxic episode on regulation of cerebral blood flow as assessed by pulsed arterial spin labelling. *NMR Biomed*. 21:696–703. doi: 10.1002/nbm.1243.

Wenzel M, Han S, Smith EH, Hoel E, Greger B, House PA, Yuste R. 2019. Reduced repertoire of cortical microstates and neuronal ensembles in medically induced loss of consciousness. *Cell Syst*. 8:467–474.e4. doi: 10.1016/j.cels.2019.03.007.

Wise RG, Ide K, Poulin MJ, Tracey I. 2004. Resting fluctuations in arterial carbon dioxide induce significant low frequency variations in BOLD signal. *Neuroimage*. 21:1652–1664. doi: 10.1016/j.neuroimage.2003.11.025.

Yamada Y, Matsumoto Y, Okahara N, Mikoshiba K. 2016. Chronic multiscale imaging of neuronal activity in the awake common marmoset. *Sci Rep*. 6:35722. doi: 10.1038/srep35722.

Zhang D, Snyder AZ, Fox MD, Sansbury MW, Shimony JS, Raichle ME. 2008. Intrinsic functional relations between human cerebral cortex and thalamus. *J Neurophysiol*. 100:1740–1748. doi: 10.1152/jn.90463.2008.

Zou Q, Long X, Zuo X, Yan C, Zhu C, Yang Y, Liu D, He Y, Zang Y. 2009. Functional connectivity between the thalamus and visual cortex under eyes closed and eyes open conditions: a resting-state fMRI study. *Hum Brain Mapp*. 30:3066–3078. doi: 10.1002/hbm.20728.